HERA-B Note 01-066 RICH 01-017

Unified Approach to Particle Identification Using the HERA-B *RICH*[*]

R.F. Schwitters

May, 2001

1 Introduction

This note outlines an approach for optimizing the particle-identification capabilities of detectors such as HERA-B by appropriately combining information from a ring-imaging Čerenkov detector (*RICH*) and a charged-particle tracking system. The proposed algorithm is based on experience gained with the HERA-B *RICH* "stand-alone" ring-finding algorithm [1, 2], where the resolution on ring center location (post-magnet track direction) is comparable to or exceeds what is possible from the charged-particle tracking system. This approach is "unified" in two senses: 1) the algorithm treats measurement errors from the two detector systems in a common way and 2) it seeks optimal particle-identification information across the "*r2p2* plot", from the high-momentum "overlap" region (where rings from different particle types have nearly the same Čerenkov angle) to the "threshold" region (momenta where particles may be near or below Čerenkov threshold).

The design performance of the HERA-B *RICH* was confirmed in studies [3] of 1999 data when a 50-50% mixture of C_4F_{10} and N_2 was used for the Čerenkov radiator. When pure C_4F_{10} became available in 2000, the system did not achieve the full improvement in Čerenkov-angle ($\theta_{\check{C}}$) resolution that was expected on the basis of the substantially increased photon statistics from the pure radiator material. At the same time, the frequency of background photon hits increased because of the larger yield from pure C_4F_{10} radiator and because of increased numbers of e^+e^- pairs created by

[*]This note is based on a talk given at the HERA-B *RICH* group meeting in Barcelona in October, 2000. The author wishes to thank Denis Dujmic, Reinhard Eckmann and Kim Hoejeong for helpful discussions.

gamma ray conversions in material up-stream of the *RICH*. It seems likely that background photon hits are limiting presently achievable resolutions for $\theta_{\check{C}}$ and ring center coordinates. Furthermore, monte carlo studies and event data indicate that only about one-half the number of hit cells can be attributed to identified Čerenkov rings.

The importance of background hits forces a detailed re-evaluation of the reconstruction/identification strategies to be used. In cases of relatively high momentum tracks—the overlap region—the best possible $\theta_{\check{C}}$ resolution is needed to distinguish between particle-type hypotheses. At lower momenta where certain particle hypotheses may be near or below Čerenkov threshold—the threshold region—every effort must be taken to eliminate backgrounds. Again, good resolution in $\theta_{\check{C}}$ can be crucial.

The excellent angular resolution of the HERA-B *RICH* permits measurements of ring parameters (radius and center coordinates) of comparable or greater accuracy than what can be predicted by the tracking system. Therefore a key ingredient in the approach suggested here is to fit for ring parameters using combined *RICH* and tracking information to obtain the best possible $\theta_{\check{C}}$ resolution. The second ingredient is an iterative algorithm to make provisional particle-ID determinations available for estimating backgrounds from rings near the ring being fitted.

When backgrounds are relatively small and the tracking resolution exceeds what is possible by stand-alone ring fitting, algorithms such as `RITER` [4] and `RIRE` [5] developed for the HERA-B *RICH* can be expected to perform satisfactorily. These algorithms are based on "classic" approaches [6, 7, 8] developed for other *RICH* systems. However, in situations like the present HERA-B, where there are relatively large backgrounds, not all of which can be assigned to rings, and where the tracking resolution is relatively poor, problems can arise in the application of the classic algorithms. For example, it is possible to over-estimate the background under real rings when the tracking resolution is poor [9]. If the single-photon angular resolution is artifically increased to avoid "over-subtracting" background, the signal-to-noise ratio may be decreased relative to an optimal analysis. The statistical methods developed for the classic algorithms are not necessarily appropriate to HERA-B's multi-anode photo-multipliers where overlapping rings may yield fewer total hits than when the rings do not overlap because only one hit can be registered by a given detector cell. Probabilities or likelihood functions evaluated for a given particle-ID hypothesis by the classic algorithms may have arbitrary or unphysical values when there is true ambiguity in the underlying data. For these reasons and more, it is appropriate to review critically the statistical basis and overall approach to particle-ID

using the HERA-B *RICH*.

2 Unified Likelihood Function

The elements of the unified approach are:

1. For each particle mass hypothesis *above* Čerenkov threshold, determine a search region in the *RICH* image plane for fitting the parameters of a "signal" ring, its neighboring background and the background level needed to describe hits in the search area assuming no actual ring is present. The area A_h of the search region should be chosen to optimize signal/background, depending on location within the *r2p2* plot.

2. Construct a negative-log-likelihood function assuming *Poisson* statistics for the hit-cell probabilities and Gaussian errors in track momentum and direction. The Poisson portion of the likelihood function has the form [10, 11]:

$$-\ln \mathcal{L}_{\text{Poisson}} = \sum_{\substack{\text{all}\\ \text{cells}}} \lambda_i \; - \sum_{\substack{\text{hit}\\ \text{cells}}} \ln(\lambda_i) \tag{1}$$

   where the λ_i represent the expected mean number of photons striking the i-th cell from all sources, signal and background.

   The contributions to the likelihood from tracking information are incorporated into the likelihood function by:

$$-\ln \mathcal{L} \; = -\ln \mathcal{L}_{\text{Poisson}} + \frac{1}{2}\left(\chi^2_p + \chi^2_{t_x} + \chi^2_{t_y}\right) \tag{2}$$

   where the various χ^2 represent squares of the deviations between track values and ring values of momenta and track direction parameters, normalized to the respective estimated errors that derive from tracking.

3. Determine the "background likelihood" $\mathcal{L}_{\text{B}}$ for the search area by assuming no signal ring is present.

4. Determine the maximum likelihood by finding ring and background parameters that minimize $-\ln \mathcal{L}$. The quantity $\mathcal{L}_{\text{max}}/\mathcal{L}_{\text{B}}$ is a measure of the *significance* that the fitted ring parameters represent a true Čerenkov ring. This and other measures of significance are used to identify the most-likely particle type or types that could have yielded the observed pattern of tracking and *RICH* information.

5. Iterate this process over valid tracks to determine the background weights that should be assigned to hits that may be shared by more than one Čerenkov ring [12].

In the following section, details of the signal component of the λ_i—the radial distribution of Čerenkov photons—are discussed. The next section gives explicit expressions for $-\ln \mathcal{L}$. How well a given hypothesis is represented by the data and fitting algorithms is the subject of the section on significance of the resulting fits. The next section discusses approximations that may be helpful in developing efficient computer algorithms for carrying out this program.

Monte carlo simulations, described in Sec. 7, give insight to the methods developed here. In particular, it may be desirable to "soften" the track momentum constraint just proposed. The expected form of distribution functions for particle bands on the *r2p2* plot is discussed in the next section. Section 9 describes a proposed particle ID algorithm that uses the results of the likelihood fits developed here. The final section summarizes our conclusions.

3 Radial Distribution

The most important quantity in determining which hit cells belong to rings and which are background is the expected radial distribution of photon hits. The mean radius r_c* is the average Čerenkov angle $\theta_{\check{C}}$, which can be related to particle masses and momenta by the following useful approximation derived from the Čerenkov relation [3]:

$$r_c^2 = \langle \theta_{\check{C}} \rangle^2 \approx r_0^2 - \frac{m^2}{p^2} \tag{3}$$

where r_0 is the limiting value of Čerenkov angle for $\beta \to 1$.

The angle-to-point optics conventionally employed in *RICH* detectors map directions of Čerenkov photons to rings on the detector surface which are centered on what would be the direction of the parent track. The term "radial distribution" is used here to describe $\theta_{\check{C}}$ distributions for detected Čerenkov photons. Ref. [13] describes how spherical aberrations in actual detector systems generally result in elliptical patterns of photon hits. Such ellipses can be corrected to equivalent circular patterns by using knowledge

*Measured in units of the focal-length of the ring-imaging optics.

of the trajectory of the parent particle as it passes through the radiator vessel. In what follows, it is assumed that appropriate optical corrections have been applied so that *circular* patterns among the photon hits are what is sought for purposes of particle-identification; the *centers* of corrected circles correspond to *directions* of the parent tracks.

The average intensity $I(x', y')$ of Čerenkov photons for a given ring is defined to be the mean number of detected photons $\bar{N}_\gamma$ per unit area $\mathcal{A}$ of the detector image plane evaluated at the horizontal, vertical angular coordinates x', y'. Under the assumptions of circular rings used here, the intensity can be expressed as:

$$I(x', y') \equiv \frac{\mathrm{d}\bar{N}_\gamma}{\mathrm{d}\mathcal{A}} = \frac{\bar{N}_\gamma(r_c)}{2\pi} f(r) \tag{4}$$

where r is the radial angular coordinate appropriate to the detector image plane. The function $f(r)$ is called the "radial distribution" and $\bar{N}_\gamma(r_c)$ is the mean total number of photons expected for a Čerenkov ring of mean radius r_c. The radial distribution function has the following general properties:

$$\begin{aligned} \int_0^\infty f(r)\, r\, \mathrm{d}r &= 1 \\ \int_0^\infty f(r)\, r^2\, \mathrm{d}r &= r_c \\ f'(0) &= 0 \end{aligned} \tag{5}$$

Most analyses—ours included—treat the radial distribution as having a Gaussian shape. Ideally, all Čerenkov photons are emitted at a fixed angle with respect to the parent particle direction—*the* Čerenkov angle—and the corresponding radial distribution is a δ-function at $\theta_{\check{C}}$. A non-zero width in the radial hit distribution arises from several sources:

1. multiple-coulomb scattering of radiating particle inside the RICH radiator
2. the distribution in $\theta_{\check{C}}$ of radiated photons due to dispersion in the radiator gas
3. the wavelength-dependence of the photon detection efficiency
4. focusing properties of the RICH

5. optical errors and misalignments in the RICH optical components and photon detectors

6. finite granularity and shape of the photon detector cells

The true radial shape will not be exactly Gaussian, but in many practical cases, it can be approximated by a Gaussian distribution. In what follows, we describe some of mechanisms for broadening the radial distribution of Čerenkov rings and estimate the resulting widths to be expected in the case of the HERA-B *RICH*.

3.1 Multiple-coulomb Scattering

Multiple-coulomb scattering of the parent particle *within* the Čerenkov radiator material will "blur" the detected ring. As described in Ref. [3], the RMS contribution of multiple-coulomb scattering to the single-hit radial error $\delta_{\rm ms}$ can be written:*

$$\delta_{\rm ms} = \frac{1}{\sqrt{2}} \left(\frac{p_{\rm ms}}{p}\right) \sqrt{\frac{T}{X_0}} \tag{6}$$

where T/X_0 is the radiator length in units of radiation-length of the radiator material, $p_{\rm ms} = 13.6\,{\rm MeV/c}$, and p is the momentum of the parent particle.

The thickness of the HERA-B *RICH* radiator corresponds to $T/X_0 = 7.6\%$ for pure C_4F_{10} and $T/X_0 = 0.9\%$ for pure N_2. Thus, the blurring of Čerenkov rings by multiple-coulomb scattering of particles in C_4F_{10} radiator is negligible ($\delta_{\rm ms} < 0.2$ mrad) when $p > 15$ GeV/c; $\delta_{\rm ms} = 0.4$ mrad is comparable to dispersion or the RMS effect of finite granularity when $p \approx 8$ GeV/c. Significant blurring occurs for rings associated with e^+e^- pairs created by post-magnet conversions of gamma rays where typical momenta are $p \ll 1$ GeV/c.

3.2 Dispersion

A calculation of the $\theta_{\check{C}}$ distribution produced by a high-momentum ($\beta \to 1$) particle radiating in pure C_4F_{10}, convolved with the wavelength-dependent photon collection/detection efficiency of the HERA-B *RICH*, is shown in Fig. 1. The distribution is non-Gaussian with an RMS spread $\sigma_{\rm d} = 0.34$mrad. A Gaussian distribution with the same RMS and mean photon yield is also plotted in the figure.

*The expression for multiple-coulomb scattering given in Ref. [3] is too small by a factor of $\sqrt{2}$. The author thanks Kim Hojeong and Denis Dujmic for pointing out this error.

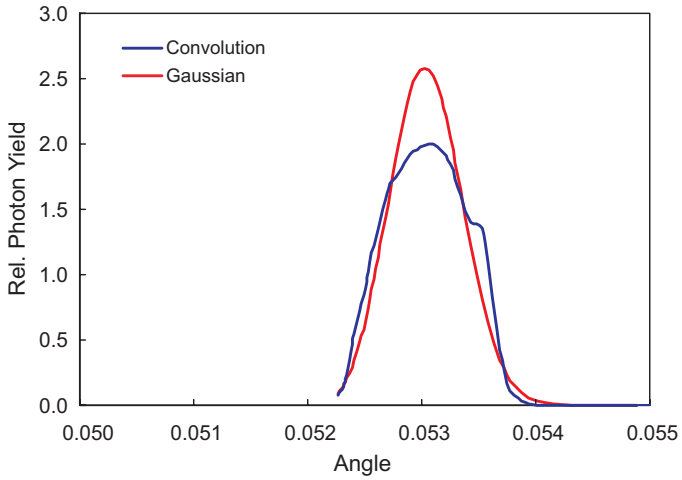

Figure 1: Blue curve: a calculation of the expected Čerenkov-angle distribution of photons detected with the HERA-B *RICH*. The "shoulder" on the right side is due to the absorption properties of the lenses used for collecting and imaging light onto photomultipliers. Red curve: a Gaussian distribution with the same mean and standard-deviation ($\sigma_{\rm d} = 0.34$ mrad).

The mean number of detected photons $\bar{N}_\gamma = 35$ found in the above calculation is in excellent agreement with measurements [3] of the HERA-B *RICH* performance.

3.3 Optical Errors

Optical errors arise from several sources:

- imperfections and misalignments of the spherical and planar mirrors
- uncorrectable spherical aberrations
- aberrations in the lens-based light collectors

Because Čerenkov light from a given track hits at most three spherical mirrors (and three planar mirrors), only local mirror misalignments will distort ring shapes. It is believed that all mirrors are aligned to the 0.1 mrad level or better. The largest errors in mirror optics are thought to be distortions of the planar mirrors due to their mounting and gravity, again estimated at the 0.1 mrad level. Uncorrectable aberrations are estimated from Ref. [13] to be in the range $0 - 0.3$ mrad over the acceptance employed

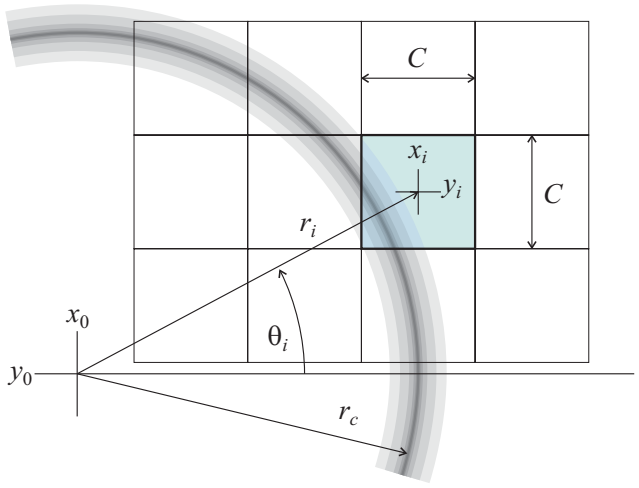

Figure 2: Schematic drawing of Čerenkov photon intensity distribution overlaying a set of detector cells.

by HERA-B. Ray-tracing studies of the lens-based light collectors indicate RMS image spreads at the level of $0.1-0.2$mrad. From these considerations, it is estimated that the uncorrelated RMS error in Čerenkov angle coming from optical errors is $\sigma_{\rm op} \sim 0.2 - 0.4$ mrad.

3.4 Detector Granularity

The mean number of Čerenkov photons λ_i falling on the i-th detector cell is related to the mean number of Čerenkov photons expected in the full ring $\bar{N}_\gamma$, the normalized radial distribution function $f(r)$ and the size and location of the cell by:

$$\begin{aligned} \lambda_i &= \frac{\bar{N}_\gamma}{2\pi} \iint\limits_{\rm cell} f(r)\ {\rm d}x\,{\rm d}y \qquad (7) \\ r &= \sqrt{(x + x_i - x_0)^2 + (y + y_i - y_0)^2} \end{aligned}$$

The coordinates of the center of cell i are given by x_i, y_i; those of the ring center are x_0, y_0. This situation is indicated schematically in Fig. 2.

As is evident from Fig. 2, λ_i depends, in principle, on the *orientation* of the detector cell relative to the local tangent to the ring as well as the distance of the center of the cell from the ring. Rather than integrating $f(r)$ over every hit cell using numerical methods, an approximate analytic expression for λ_i was found in Ref. [14] by assuming a Gaussian form for $f(r)$

and expanding in powers of the cell-size/ring-width (C/σ) in the vicinity of the Čerenkov ring. The convergence of such an expression is questionable, but numerical integrations indicate the accuracy of this procedure is at the few-% level within several σ of typical rings. The resulting analytic expression is dominated by the result one might expect intuitively:

$$\lambda_i \approx \frac{\bar{N}_\gamma \, a_i}{(2\pi)^{3/2} \, r_c \, \sigma_i} \exp\left[-\frac{1}{2}\left(\frac{r_c - r_i}{\sigma_i}\right)^2\right] \qquad \sigma_i \equiv \sqrt{\sigma^2 + \frac{a_i}{12}} \tag{8}$$

where $a_i = C_i^2$ is the area of the hit cell, $r_c = \langle \theta_{\check{C}} \rangle$ is the mean Čerenkov angle and σ is the RMS radial width of the Čerenkov ring. As described above, σ has contributions from multiple-coulomb scattering, dispersion and optical errors, which are described by:

$$\sigma^2 = \delta_{\rm ms}^2 + \sigma_{\rm d}^2 + \sigma_{\rm op}^2 \tag{9}$$

With the estimates described here, the convolved σ's appropriate to the HERA-B *RICH* ($p > 5$ GeV/c) are $\sigma_i = 0.7$ mrad for M-16 PMT cells and $\sigma_i = 1.0$ mrad for M-4 PMT cells. These values are consistent with results from stand-alone ring fitting [3].

Orientation-dependent corrections to Eqn. 8 are of order $(C/24\sigma)^4$ and are ignored in the present analysis.

4 Detailed Formulas

In this section, equations from references and other sections of this note are reproduced with a consistent set of symbols.

4.1 Ring Parameters

In a track-based ring fitting algorithm, the first approximation to the ring radius and center location $\{r_c, x_0, y_0\}$ are given by the track momentum and direction through the *RICH*: $\{r_h, t_x, t_y\}$, where r_h depends on the mass hypothesis m_h according to:

$$r_h = \sqrt{r_0^2 - \left(\frac{m_h}{p}\right)^2} \tag{10}$$

Deviations between the maximum-likelihood fitted ring parameters and the track values are described by:

$$r_c = r_h + \epsilon \qquad x_0 = t_x + x \qquad y_0 = t_y + y \tag{11}$$

All three differences $\{\epsilon, x, y\}$ can be treated as being "small" relative to $\theta_{\check{C}}$.

The mean number of Čerenkov photons around a complete ring $\bar{N}_\gamma$ is proportional to $\theta^2_{\check{C}}$, but to an adequate approximation can be written as:

$$\bar{N}_\gamma \equiv \mathcal{N}_0 T \; r_c^2 \approx \mathcal{N}_0 T \; r_h^2 \tag{12}$$

where the parameters $\mathcal{N}_0 T$ describing the overall detection efficiency and Čerenkov photon yield of the *RICH* are defined in Ref. [11].

Using the notation of Ref. [12], the Čerenkov photon "flux" from one ring falling on a particular cell* can be written in terms of the fitting parameters $\boldsymbol{\xi} = \{\epsilon, x, y\}$ and track-based quantities $\{r_h, t_x, t_y\}$ as:

$$\begin{aligned} \phi_i(\boldsymbol{\xi}) &= \frac{r_h}{\sigma_i} \; \exp\left[-\frac{1}{2}\left(\frac{r_h - r_i + \epsilon + \boldsymbol{x}\cdot\hat{\boldsymbol{u}}_i}{\sigma_i}\right)^2\right] \\ \boldsymbol{x} &= x\,\hat{\boldsymbol{x}} + y\,\hat{\boldsymbol{y}} \qquad \hat{\boldsymbol{u}}_i = \frac{(x_i - t_x)}{r_i}\,\hat{\boldsymbol{x}} + \frac{(y_i - t_y)}{r_i}\,\hat{\boldsymbol{y}} \\ r_i &= \sqrt{(x_i - t_x)^2 + (y_i - t_y)^2} \end{aligned} \tag{13}$$

where x_i, y_i are the coordinates of the center of the hit cell; $\hat{\boldsymbol{x}}, \hat{\boldsymbol{y}}$ are unit vectors in the horizontal, vertical directions.

The ring parameters $\boldsymbol{\xi}$ also enter the χ^2 terms introduced into the likelihood function to account for tracking errors. These terms are given by:

$$\chi^2_p = r_h^2 \left(\frac{p}{m_h}\right)^4 \left(\frac{\epsilon}{\delta p/p}\right)^2 \qquad \chi^2_{t_x} = \left(\frac{x}{\sigma_{x'}}\right)^2 \qquad \chi^2_{t_y} = \left(\frac{y}{\sigma_{y'}}\right)^2 \tag{14}$$

where $\delta p/p$ is the estimated momentum resolution for the track and $\sigma_{x'}, \sigma_{y'}$ are the angular tracking errors in the horizontal and vertical planes, respectively.

With present HERA-B tracking, the errors on predicted ring centers $(\sigma_{x'}, \sigma_{y'})$ are of order $(1, \text{few})$ mrad, respectively, which are comparable to or somewhat worse than the center resolution that can be achieved by standalone ring finding [3]. Momentum errors contribute to an uncertainty $\sigma_h \equiv (\delta\, p/p)(m_h/p)^2/r_h$ in the predicted ring radius, as described by the χ^2_p term above. Present momentum errors from HERA-B tracking give typical radius errors of order a few tenths of a mrad which are comparable to the standalone radius determination.

*In *RICH* systems such as HERA-B's, where optics and photon detectors are split, there is a subtlety in computing the flux for rings that share hits across the split detectors. The flux described here must be properly apportioned across the split to avoid double-counting.

4.2 Background Parameters

Following Refs. [11, 12], the mean number of background photons b_i falling on the i-th cell of the search space is given by:

$$b_i = \frac{\mathcal{N}_0 T}{(2\pi)^{3/2}}\, a_i\, [\, R_{\rm B} + \beta_i \,] \tag{15}$$

where $R_{\rm B}$ is a parameter describing uniform background hits not associated with other rings and β_i is the Čerenkov photon flux due to *other* rings. $R_{\rm B}$ is an additional fitting parameter which, along with $\boldsymbol{\xi}$, is used to minimize $-\ln \mathcal{L}$.

For the initial ring-finding iteration, there is no information on overlapping rings and the values $\beta_i = 0$ should be used. After a provisional set of rings is determined for the event, the influence of overlapping rings is calculated using Eqn. 13 to give:

$$\beta_i = \sum_{\substack{\text{selected}\\ \text{rings}}} \frac{R_{\rm t}}{\sigma_i}\, \exp\left[-\frac{1}{2}\left(\frac{R_i - R_{\rm t}}{\sigma_i}\right)^2\right] \tag{16}$$

where the indicated sum is over the selected background rings (labeled by the index t), $R_{\rm t}$ is the radius of the ring associated with track t and R_i is the distance of the i-th cell from the center of the background ring*. It is an interesting fact that the mean of the *total* number of photons expected from background rings overlapping the search area is not needed in this algorithm because it cancels in $\ln \mathcal{L}/\mathcal{L}_{\rm B}$; only the fluxes evaluated for cells actually hit, the β_i, are required.

In the case where there is no ring present in the search area, $R_{\rm B}$ will have a particular value which is denoted by $\tilde{R}_{\rm B}$. As shown below, $\tilde{R}_{\rm B}$ enters critically into the relative likelihood function $\mathcal{L}/\mathcal{L}_{\rm B}$, the actual quantity to be maximized in the unified algorithm described here. $\tilde{R}_{\rm B}$ can be determined directly from the data without fitting for the other ring and background parameters; it is a root of the equation:

$$\frac{\mathcal{N}_0 T\ A_h}{(2\pi)^{3/2}} = \sum_{\substack{\text{hit}\\ \text{cells}}} \frac{1}{\tilde{R}_{\rm B} + \beta_i} \tag{17}$$

where A_h is the total area of the search space.

*Note that different optical corrections should be applied to the cell when computing its background flux because, in general, spherical aberrations differ for different tracks.

4.3 Total Number of Photons

The first term in the basic Poisson likelihood function, Eqn. 1, represents the mean of the total number of all photons—signal plus background—that would be detected in the search area, assuming detectors of infinite granularity. This term has contributions from three sources: 1) photons from the ring being fitted in the search area (assuming the correct hypothesis has been chosen); 2) background photons from segments of other rings which intersect the search area; and 3) background photons that cannot be assigned to rings.

When the search area is near the center or boundaries of acceptance, corrections need to be applied for the fraction of the ring azimuth that falls on active detectors. This is called the "shadowing correction"; it arises from actual shadowing by the proton or electron beam shrouds or cutoff of acceptance due to finite detector coverage. The corresponding shadowing corrections for background rings intersecting the search area are not needed because they contribute equal amounts to $\mathcal{L}$ and $\mathcal{L}_{\rm B}$ and, therefore, cancel in $\ln \mathcal{L}/\mathcal{L}_{\rm B}$ as mentioned previously.

4.4 Likelihood Function

Collecting everything together, the actual function to be minimized by varying $\boldsymbol{\xi}, R_{\rm B}$ is:

$$
\begin{aligned}
-\ln \frac{\mathcal{L}(\boldsymbol{\xi}, R_{\rm B})}{\mathcal{L}_{\rm B}} \;\; = \;\; & \mathcal{N}_0 T \left[f_{\rm s}\, r_h^2 + \frac{A_h}{(2\pi)^{3/2}} (R_{\rm B} - \tilde{R}_{\rm B}) \right] \\
& - \sum_{\substack{\text{hit} \\ \text{cells}}} \ln \left[\frac{\phi_i(\boldsymbol{\xi}) + R_{\rm B} + \beta_i}{\tilde{R}_{\rm B} + \beta_i} \right] \\
& + \frac{1}{2} \left[\left(\frac{\epsilon}{\sigma_h} \right)^2 + \left(\frac{x}{\sigma_{x'}} \right)^2 + \left(\frac{y}{\sigma_{y'}} \right)^2 \right]
\end{aligned}
\tag{18}
$$

where $f_{\rm s}$ is the shadowing correction for the hypothetical ring.*. Generally, the shadowing correction plays no role in fitting for optimum ring parameters, but it is important for computing the value of $\ln(\mathcal{L}_{\rm max}/\mathcal{L}_{\rm B})$ for use in comparing different hypotheses or applying cuts (see Sec. 9) when the search

*In principle, the flux at each hit cell ϕ_i may suffer some loss due to shadowing. It is assumed here that hit cells are not shadowed, only that some sections of rings are lost. A related issue, mentioned previously, is the apportionment of flux between the two sets of photo-detectors in a system with split optics.

area is near the acceptance boundary or could be shadowed by beam-pipe shrouds.

The three lines of Eqn. 18 correspond respectively to 1) the mean of the total number of photons expected to be present, 2) the weights to be assigned to hit cells and 3) the χ^2 terms which describe the constraints provided by the tracking information.

For completeness, the expression for the ring flux is repeated here:

$$\phi_i(\boldsymbol{\xi}) = \frac{r_h}{\sigma_i} \exp\left[-\frac{1}{2}\left(\frac{r_h - r_i + \epsilon + \boldsymbol{x}\cdot\hat{\boldsymbol{u}}_i}{\sigma_i}\right)^2\right]$$

5 Significance of the Resulting Fit

The likelihood ratio $\mathcal{L}_{\max}/\mathcal{L}_{\rm B}$ evaluated at the best-fit values for the parameters $\boldsymbol{\xi}, R_{\rm B}$ certainly carries information about the quality of the fit to the ring-plus-background hypothesis; exactly what it can tell us of a quantitative nature about the significance* of the corresponding particle identification hypothesis is obscure. Any given configuration of photon hits for a true ring with background has a tiny probability because of the large number of cells in a typical search area and the small probability that a particular cell actually triggers, even if it lies close to the Čerenkov ring. There are large numbers of equivalent or nearly equivalent configurations of hit cells for any actual ring/background pattern. Short of a complete understanding of the "statistical mechanics" of these equivalent configurations, it is not clear how, for example, the values of $\mathcal{L}_{\max}/\mathcal{L}_{\rm B}$ for different particle ID hypotheses on a given track relate to the true particle ID. Monte carlo studies, described in Sec. 7, illuminate the role of $\ln(\mathcal{L}_{\max}/\mathcal{L}_{\rm B})$ as a measure of significance.

The relatively sharp, bright† Čerenkov rings encountered with the HERA-B *RICH* can give rise to numerous false minima in $-\ln\mathcal{L}$. This happens because the contribution of a single hit cell to $-\ln\mathcal{L}$ can vary by several units depending on whether the best-fit ring passes near to the center or to an edge of the cell. By comparison, a 1-σ change in a fitting parameter from the optimum value should only change $-\ln\mathcal{L}$ by one-half unit. In terms of the Δ parameter (see footnote below), the weight of a cell lying centered on a Čerenkov ring is $\frac{1}{2}(\Delta/\sigma)^2$ compared to one centered Δ away from a

*Ref. [11] defines a significance $\mathcal{S}$ by a gaussian-like relationship $\mathcal{S}^2/2 \equiv \ln(\mathcal{L}_{\max}/\mathcal{L}_{\rm B})$

†Following [11], we define the ring "brightness" as r_h/σ. The ring brightness can be related to the average background level R_B by the parameter Δ which is defined as the radial distance from the circle of maximum ring intensity to the contours where the ring intensity equals the uniform background intensity; Δ is given by $(\Delta/\sigma)^2 = 2\ln(r_h/R_B\cdot\sigma)$.

ring. For typical background levels, $\Delta \sim 2-3\,\sigma$, which is comparable to or smaller than the size of a single detector cell. Thus, the finite granularity of devices such as the HERA-B *RICH*, when confronted by significant background occupancies, increases the noise or structure in $-\ln\mathcal{L}$, further complicating the interpretation of likelihood ratios for determining goodness of particular fits.

The value of the best-fit likelihood ratio can be crudely estimated in a "toy" model [11] where there are S signal hits (fully contained within $\pm\Delta$ of the best-fit radius) from a ring of radius r_h and B background hits distributed uniformly over the search area (no intersecting background rings):

$$\begin{aligned}\ln\frac{\mathcal{L}_{\max}}{\mathcal{L}_{\rm B}} \;\approx\; & \frac{1}{2}\,S\left[1+\left(\frac{\Delta}{\sigma}\right)^2\right]-\bar{N}_\gamma(r_h)+(S+B)\ln\left(\frac{B}{S+B}\right)\\ & +\frac{2}{3}\frac{\bar{N}_\gamma}{\sqrt{2\pi}}\left(\frac{\Delta}{\sigma}\right)^3\exp-\frac{1}{2}\left(\frac{\Delta}{\sigma}\right)^2 \;-\; \frac{1}{2}\chi^2(\boldsymbol{\xi})\end{aligned} \tag{19}$$

While one can understand qualitatively the appearance of the various terms in Eqn. 19 and argue their plausible utility as a measure of goodness of fit, the complexity of this expression and its inclusion of vestiges of the large numbers of equivalent configurations of hits, mentioned previously, do not seem to warrant the effort. In addition to using the likelihood ratio as a measure of goodness of fit, we suggest three more conventional measures which could be used collectively in a multivariate selection process:

1. A comparison of the number of signal events S determined from the fit with the number of photons expected $\bar{N}_\gamma$.

2. The spread in radial locations of hits about the best-fit ring.

3. The quality of matching between the best-fit ring and tracking information as expressed by the $\chi^2(\boldsymbol{\xi})$ terms in Eqn. 18.

As defined, the quantity $\tilde{R}_{\rm B}$ is proportional to the total number of hits *not* associated with intersecting background rings while $R_{\rm B}$ is proportional to the expected number of background hits not associated with any rings. Therefore, the weighted* number of signal hits S present in a given fit can be found from:

$$S=\frac{\mathcal{N}_0 T\;A_h}{(2\pi)^{3/2}}\left(\tilde{R}_{\rm B}-R_{\rm B}\right) \tag{20}$$

* "Weighted" refers to the effect of overlapping rings and smooth background in the search area which diminishes S according to the relative background flux.

The estimated error δS on the number of signal hits is properly computed from the fitted error $\delta R_{\rm B}$ in $R_{\rm B}$ alone; statistical errors in $\tilde{R}_{\rm B}$ are correlated with $R_{\rm B}$ and need not be included in the estimate of δS. If intersecting background rings are not being re-weighted, i.e. all $\beta_i = 0$, then $S = \mathcal{W}$, where $\mathcal{W}$ is the total signal flux weight for the ensemble of hit cells, defined later in Eqn. 23; there are small corrections to this expression when $\beta_i \neq 0$.

A χ^2-like measure of the agreement between observed photon yield and that expected can be defined as:

$$\mathcal{N}^2 \equiv \frac{\left(S - f_{\rm s}\bar{N}_\gamma\right)^2}{(\delta S)^2 + f_{\rm s}\bar{N}_\gamma} \tag{21}$$

A measure of how well the pattern of hits represents a Čerenkov ring can be found by computing the mean-square deviation of signal-weighted hits from the best-fit circle. While such quantities are likely to be biased estimators in the statistical sense, we suggest the following quantity to represent the quality of the ring fit:

$$\mathcal{D}^2 = \left\langle \left(\frac{r_h - r_i + \epsilon + \boldsymbol{x}\cdot\hat{\boldsymbol{u}}_i}{\sigma_i} \right)^2 \right\rangle_{\rm f} \tag{22}$$

where the signal flux-weighted average is defined by:

$$\begin{aligned} \langle A \rangle_{\rm f} &\equiv \frac{1}{\mathcal{W}} \sum_{\substack{\rm hit \\ \rm cells}} A_i \left(\frac{\phi_i}{\phi_i + R_{\rm B} + \beta_i} \right) \\ \mathcal{W} &= \sum_{\substack{\rm hit \\ \rm cells}} \left(\frac{\phi_i}{\phi_i + R_{\rm B} + \beta_i} \right) \end{aligned} \tag{23}$$

where ϕ_i is evaluated using best-fit parameters $\boldsymbol{\xi}$.

A strong ring signal should give a distribution in $\mathcal{D}^2$ similar to that of χ^2/n, while pure background will have* $\langle \mathcal{D}^2 \rangle \sim \frac{1}{3}(\Delta/\sigma)^2$. In situations of relatively small background, real rings should populate distinctly different values of $\mathcal{D}^2$ compared to only background.

*For these estimates, we use the Δ parameter introduced previously to describe the relative background flux. The definition of Δ/σ depends weakly on cell size through $[\ln(\sigma_i)]^{1/2}$. A "typical" cell size should be chosen for estimates, representative of the majority of cells contributing to the ring.

The signal-to-noise† ratio of hits contributing to $\mathcal{D}^2$—and to the determination of ring parameters—can be estimated by:

$$\mathrm{S/N} \approx \sqrt{\frac{\pi}{2}} \frac{S}{\bar{N}_\gamma(r_h)} \frac{\exp \frac{1}{2}\left(\frac{\Delta}{\sigma}\right)^2}{(\Delta/\sigma)} \tag{24}$$

The χ^2 terms which describe the matching of the fitted ring to the track information can be incorporated into a quality factor χ^2_{t} defined by:

$$\chi^2_{\mathrm{t}} \equiv r_h^2 \left(\frac{p}{m_h}\right)^4 \left(\frac{\epsilon}{\delta p/p}\right)^2 + \left(\frac{x}{\sigma_{x'}}\right)^2 + \left(\frac{y}{\sigma_{y'}}\right)^2 \tag{25}$$

Of the three measures proposed for describing the quality of the fit and for discriminating between competing particle-ID hypotheses, the χ^2_{t} term is expected to be the most incisive because of the high accuracy with which *RICH* systems are capable of determining Čerenkov ring radii. $\mathcal{D}^2$, which is largely determined by the RMS spread in hit locations about the fitted ring, cannot be expected to distinguish clearly between signal and background in most instances, but it should indicate poorly fitted rings. Statistical fluctuations will dominate distributions of $\mathcal{N}^2$ because we are dealing with small numbers of signal hits, at best in the range 15 - 35. Despite these defects in $\mathcal{D}^2$ and $\mathcal{N}^2$, they may be helpful for ensuring consistency among fit solutions even if actual hypothesis selections are made primarily with χ^2_{t}.

6 Approximate Solutions

Substantial computing is required to perform the iterated, non-linear fits implied by the methods described here. Each hypothesis examined for each track involves four fitting parameters $\boldsymbol{\xi}, R_{\mathrm{B}}$. Each track has the additional pure-background parameter $\tilde{R}_{\mathrm{B}}$ and the entire set of tracks in an event is iterated to "re-weight" hits that might be shared by overlapping rings. Clearly, efficient algorithms are required to carry out the necessary computations. Here we examine the equations to be solved in order to find features that might be exploited to improve computational performance. These approaches must still be verified, however, through detailed performance studies.

†In this context, "noise" refers to the number of background hits within $\pm\Delta$ of the fitted Čerenkov radius.

As developed here, the condition for maximizing $\mathcal{L}$ for the *ring* parameters $\boldsymbol{\xi}$ corresponds to a linearized, least-square circle-fit involving flux-weighted residuals. In the approximation that the flux factors ϕ_i and $R_{\rm B}$ are not varied, this problem is solved by conventional techniques. The *background* parameter $R_{\rm B}$ is a solution of an equation of quite a different character:

$$\frac{\mathcal{N}_0 T\ A_h}{(2\pi)^{3/2}} = \sum_{\substack{\rm hit \\ \rm cells}} \frac{1}{R_{\rm B} + \phi_i(\boldsymbol{\xi}) + \beta_i} \tag{26}$$

which is essentially the same as Eqn. 17, but with the inclusion of the signal flux ϕ_i for each hit cell. Because typical Čerenkov rings, signal or background, are so bright, their fluxes are either quite large relative to $R_{\rm B}$ or are small. Thus, a simple algorithm that gives an approximate solution is to count the number of hits N_h only if the ring fluxes ϕ_i, β_i are smaller than some trial value for $R_{\rm B}$, say $\tilde{R}_{\rm B}$. Then, the approximate solution is:

$$R_{\rm B}^{(0)} \approx \frac{N_h(\phi_i + \beta_i < \tilde{R}_{\rm B})}{A} \qquad A = \frac{\mathcal{N}_0 T\ A_h}{(2\pi)^{3/2}} \tag{27}$$

In the same way, a first approximation to $\tilde{R}_{\rm B}$ can be found by:

$$\tilde{R}_{\rm B}^{(0)} \approx \frac{N_h(\beta_i < N_{\rm tot}/A)}{A} \tag{28}$$

where $N_{\rm tot}$ is the total number of hit cells in the search space. Standard techniques can be used to compute the next-order corrections to these expressions. We can estimate the statistical error $\delta R_{\rm B}$ in the determination of $R_{\rm B}$, neglecting correlations with the ring parameters, by considering only the diagonal element of the covariance matrix. The result is:

$$\delta R_{\rm B}^{(0)} \approx \left[\sum_{\substack{\rm hit \\ \rm cells}} \frac{1}{(R_{\rm B} + \phi_i + \beta_i)^2} \right]^{-\frac{1}{2}} \tag{29}$$

We assume that the ring flux parameters ϕ_i in the preceding are computed using ring parameters derived from the tracking information alone. The first approximation to the deviations $\boldsymbol{\xi}$ from tracking values for the ring parameters can be found from solutions to the linearized circle-fit:

$$\boldsymbol{\xi}^{(0)} = \mathcal{W}\boldsymbol{V}\boldsymbol{\rho} \tag{30}$$

where:

$$\boldsymbol{\rho} = \begin{pmatrix} \left\langle \frac{r-r_h}{\sigma^2} \right\rangle_{\mathrm{f}} \\ \left\langle u_x \left(\frac{r-r_h}{\sigma^2} \right) \right\rangle_{\mathrm{f}} \\ \left\langle u_y \left(\frac{r-r_h}{\sigma^2} \right) \right\rangle_{\mathrm{f}} \end{pmatrix} \qquad \boldsymbol{\xi} = \begin{pmatrix} \epsilon \\ x \\ y \end{pmatrix} \tag{31}$$

and the inverse-covariance matrix (for ring parameters only) is given by:

$$V^{-1} = \mathcal{W} \begin{pmatrix} \left[\left\langle \frac{1}{\sigma^2} \right\rangle_{\mathrm{f}} + \frac{1}{\mathcal{W}\sigma_h^2} \right] & \left\langle \frac{u_x}{\sigma^2} \right\rangle_{\mathrm{f}} & \left\langle \frac{u_y}{\sigma^2} \right\rangle_{\mathrm{f}} \\ \left\langle \frac{u_x}{\sigma^2} \right\rangle_{\mathrm{f}} & \left[\left\langle \frac{u_x^2}{\sigma^2} \right\rangle_{\mathrm{f}} + \frac{1}{\mathcal{W}\sigma_{x'}^2} \right] & \left\langle \frac{u_x u_y}{\sigma^2} \right\rangle_{\mathrm{f}} \\ \left\langle \frac{u_y}{\sigma^2} \right\rangle_{\mathrm{f}} & \left\langle \frac{u_x u_y}{\sigma^2} \right\rangle_{\mathrm{f}} & \left[\left\langle \frac{u_y^2}{\sigma^2} \right\rangle_{\mathrm{f}} + \frac{1}{\mathcal{W}\sigma_{y'}^2} \right] \end{pmatrix} \tag{32}$$

$\mathcal{W}$ is the sum of flux weights as defined in Eqn. 23.

One can expect that successive iterations of these linearized equations for $R_{\mathrm{B}}, \boldsymbol{\xi}$, with recomputed ring fluxes $\phi_i(\boldsymbol{\xi})$, should converge rapidly; this is confirmed in the monte carlo studies described in the next section.

7 Monte Carlo Studies

The unified fitting approach described above has been tested with monte carlo simulations. A MS Excel workbook was developed for testing the basic likelihood approach and for comparing a detailed non-linear fitting algorithm with the linearized approximations described in the previous section.

Briefly, this tool sets up an arbitrary set of particle tracks in a simplified version of the HERA-B *RICH* with photon detector cell sizes and particle tracking resolutions comparable to the HERA-B case, but with smaller acceptance and without "physics-based" event generation. Events are formed by generating photon hits according to Poisson statistics applied to the ideal tracks, while one "detected" track is chosen from the list and its momentum and direction are smeared appropriately. In addition to background hits from the other tracks, a uniform background is also simulated. The detected track momentum and direction are used to define annular search areas for hypothesis fits as described above. A typical event is shown in Fig. 3. The corresponding search area for the target track (indicated by the red circle in Fig. 3) is shown in Fig. 4.

Initial conclusions derived from our monte carlo studies are discussed in the following sub-sections.

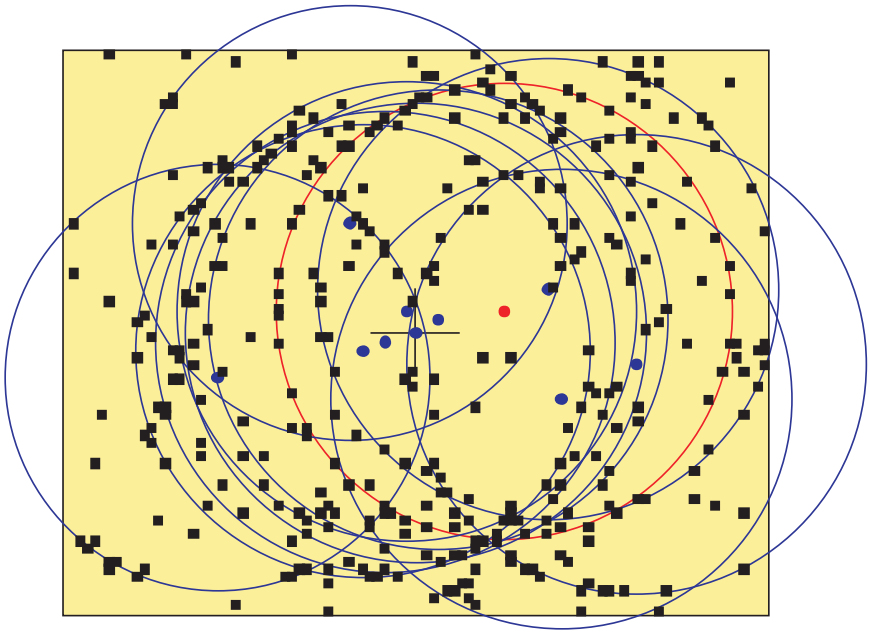

Figure 3: Photon detector image-plane view of Čerenkov photon hits from a typical monte carlo event used in the studies discussed here. Circles corresponding to expected Čerenkov rings are shown. The red ring corresponds to the target track being fitted. Width of cross at center indicates ±10mrad.

7.1 Momentum constraint on radius should be relaxed

The constraint on Čerenkov radius provided by track momentum—the ϵ/σ_h term in the χ^2 contribution to the overall likelihood function (Eqn. 18)—is especially strong, causing ring parameters to be "pulled" to a particular hypothesis, particularly in cases where bands begin to coalesce on the *r2p2* plot. This effect can be seen in Fig. 5 where the distance* D_h of the fitted ring parameters from the *r2p2* band corresponding to hypothesis h is plotted versus log-likelihood ratios for various hypotheses.

As will be discussed below in Sec. 8, the widths of *r2p2* bands can be described by a confidence-level function $\mathcal{P}(D_h) = \exp -D_h^2/2$. Therefore we expect the kind of correlation observed in Fig. 5 because when bands begin to overlap, $\ln \mathcal{L}_h/\mathcal{L}_{h'} \sim (D_{h'}^2 - D_h^2)/2 \sim -D_h(m_h^2 - m_{h'}^2)/(p^2\sigma_{\theta^2})$, where σ_{θ^2} is the estimated error on the square of the fitted Čerenkov angle.

Our monte carlo simulations show that to achieve good fits to true

*See the discussion in Sec. 8 below for the definition of and motivation for using D_h.

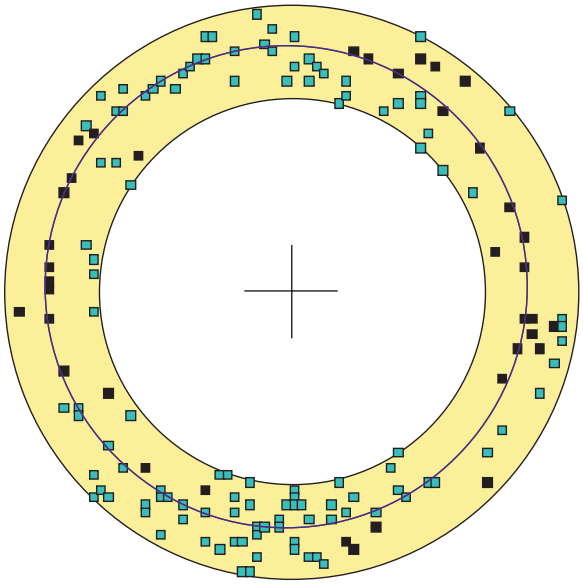

Figure 4: Search area for the target track indicated in Fig. 3 under the correct—pion, in this case—hypothesis. Hits filled in blue have substantial flux ($\beta_i \geq 10$) from background tracks. Circles corresponding to the target Čerenkov ring fitted by a full, non-linear fitting algorithm and the linearized approximation are shown. The two fits are identical within estimated errors. Width of cross at center indicates ± 10 mrad.

Čerenkov rings, it is not necessary to include the full momentum constraint in the likelihood function. A soft momentum constraint, corresponding to several mrad in Čerenkov radius, is useful in confining the fit within the selected search area and avoiding numerous false minima. When a true ring is encountered, the excellent angular resolution and statistical power of the *RICH* is sufficient to determine the ring radius to the 0.1 mrad level, even when substantial backgrounds are present. An example is shown in Fig. 6.

These results suggest that when different hypothesis bands coalesce—the "overlap" region of the *r2p2* plot—it is only necessary to perform one likelihood fit (starting at the center of the full overlapped band) to determine if a ring is present and to find its radius, as long as a soft momentum constraint is applied.

For the remainder of this note, the fits use a momentum constraint corresponding to ± 2 mrad in Čerenkov radius, which is more than an order of magnitude larger than the true momentum constraint. The results are not

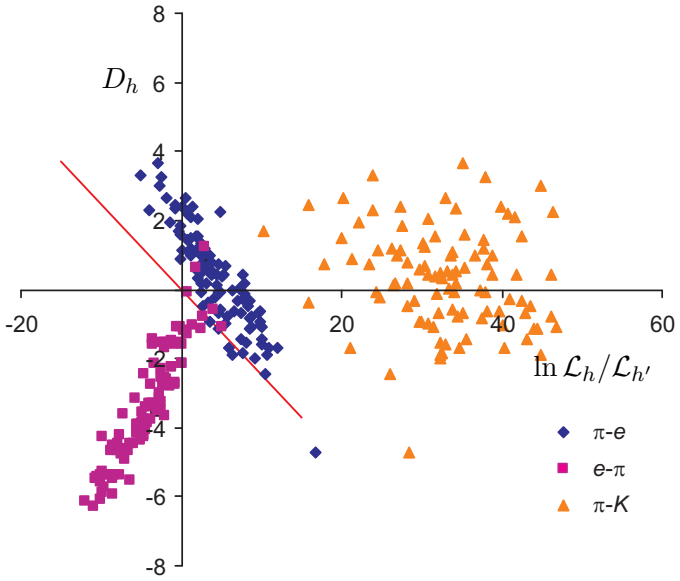

Figure 5: Results of likelihood fits for 20 GeV/c particles; the correct particle hypothesis is pion. The *r2p2* distance D_h for various hypotheses h is plotted versus the log-likelihood ratio $\ln \mathcal{L}_h/\mathcal{L}_{h'}$ to the nearby hypothesis h'. Correlations forced by the strong momentum constraint are evident between the nearby electron and pion hypotheses. The red line indicates the slope of the expected correlation for the pion hypothesis. To be included on the plot, a given point is required to have $\ln(\mathcal{L}_{\rm max}/\mathcal{L}_{\rm B}) > 2$ for h, the hypothesis being tested; there is no likelihood cut on h'.

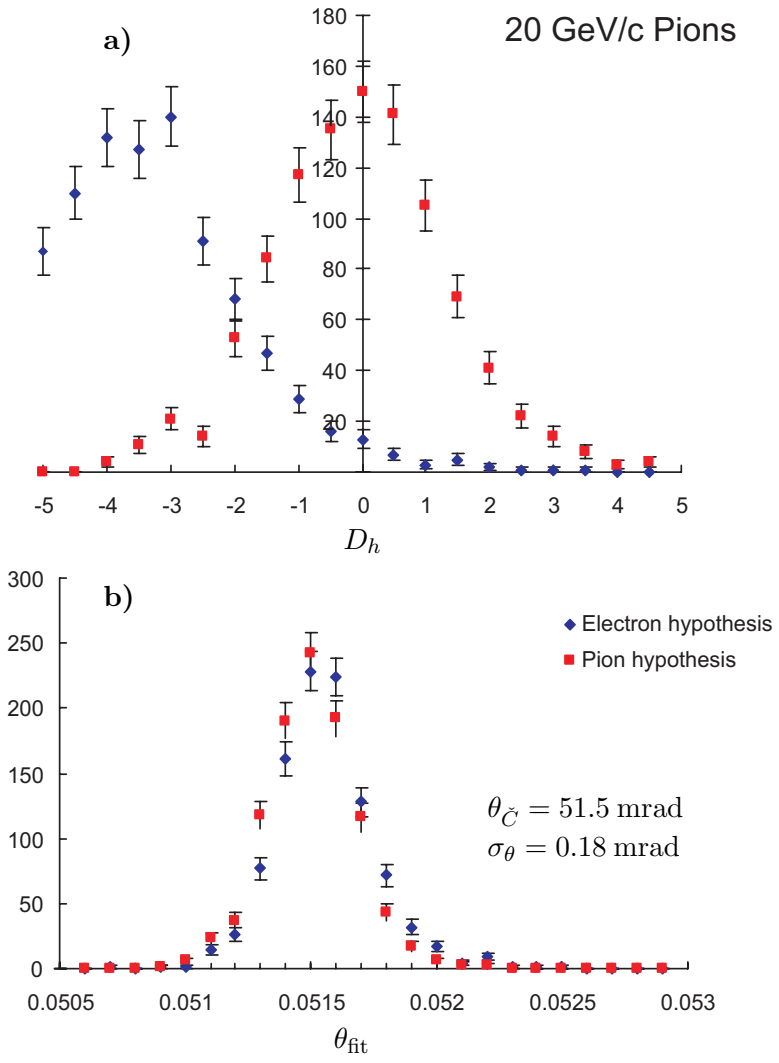

Figure 6: Results of likelihood fits using a soft momentum constraint for 20 GeV/c particles—the true particles are pions. Histogram a): number versus the *r2p2* distance D_h for pion and electron hypotheses. Histogram b): number versus fitted Čerenkov radius for pion and electron hypotheses. Fits were performed with backgrounds as depicted in Fig. 3.

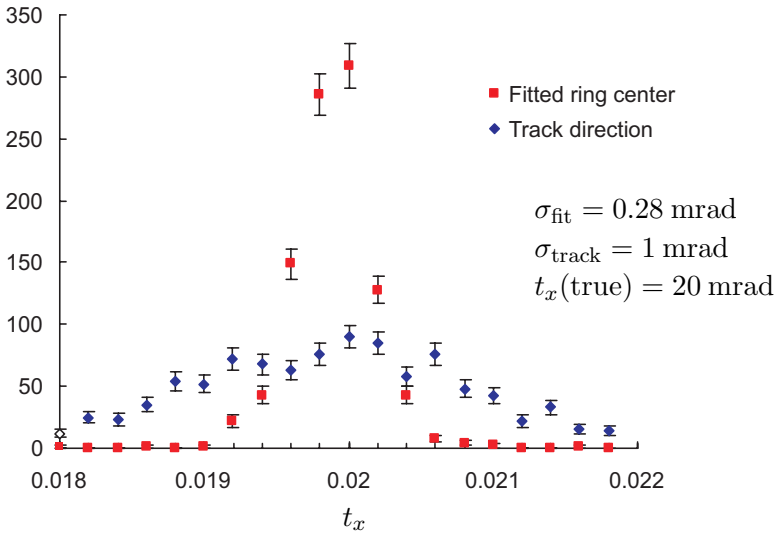

Figure 7: Histogram of horizontal track direction (ring center) t_x from likelihood fits using a soft momentum constraint for 20 GeV/c particles—the true particles are pions. Fits were performed with backgrounds as depicted in Fig. 3. Notice that the fitted resolution in one-dimension of track direction is approximately $\sqrt{2}$ times the resolution in fitted radius (see Fig. 6), as expected for rings fully contained within the *RICH* acceptance.

sensitive to the details of this soft constraint.

Most important, the ring parameters obtained from fits with the soft momentum constraint are not correlated significantly with momentum. This will be crucial to the discussion in Sec. 8 were the relative probabilities of competing hypotheses that overlap on the *r2p2* plot are considered.

Constraints imposed by track direction on the location of the ring center are helpful for convergence of the fits. The resulting ring parameters can substantially improve knowledge of the parent track direction. Fig. 7 shows the improvement to be expected for 20 GeV/c pion tracks; even greater improvement is expected in the vertical direction where the HERA-B track direction resolution is worse than 1 mrad.

7.2 $\ln(\mathcal{L}_{\rm max}/\mathcal{L}_{\rm B})$ is a useful measure of significance/goodness-of-fit

The comments in Sec. 5 notwithstanding, our monte carlo studies indicate that $\ln(\mathcal{L}_{\rm max}/\mathcal{L}_{\rm B})$ is a convenient and meaningful measure of significance

and goodness-of-fit. The other measures—χ^2, $\mathcal{D}^2$ and $\mathcal{N}^2$—suggested in the earlier discussion are strongly correlated with $\ln(\mathcal{L}_{\max}/\mathcal{L}_{\rm B})$ and do not seem to offer any particular advantages. The key point is that $\ln(\mathcal{L}_{\max}/\mathcal{L}_{\rm B})$ is a measure of the likelihood of the fitted hypothesis *relative* to that of pure background giving the configuration of hits observed in the search area.

The main difference between the two factors that make up $\ln(\mathcal{L}_{\max}/\mathcal{L}_{\rm B})$ is that $\mathcal{L}_{\max}$ includes contributions from hits related to how well they fall on the putative Čerenkov ring. These weights are offset by the expected yield of Čerenkov photons, which is *subtracted* from $\mathcal{L}_{\max}$. Even though it is nearly always possible to find a circle through hits in any search area, the number of hits close to the ring must be consistent with that expected for a real Čerenkov ring in order to have a positive value for $\ln(\mathcal{L}_{\max}/\mathcal{L}_{\rm B})$.

An example of the interplay between apparent signal and expected signal can be seen in Fig. 8. For the kinematics depicted, the pion and kaon search areas have essentially no overlap. Thus, the false hypotheses represent examples of nearly pure background, while the correct hypotheses have the signal ring and background from all the other sources. The two possibilities are cleanly separated, to the extent possible by the underlying photon statistics. In both the true and false cases, pions have slightly more significance—positive and negative—due to the larger mean number of expected hits. The impression is made stronger if the significance $\mathcal{S}$ (see footnote on page 13) is plotted. Peak values of this measure of significance have the naively expected value $\mathcal{S} \sim \sqrt{\bar{N}_\gamma}$.

These results suggest that a simple $\ln(\mathcal{L}_{\max}/\mathcal{L}_{\rm B}) > 0$ test may be sufficient to indicate whether or not the particular *r2p2* band being tested does or does not have a ring present. Such a cut will not, of course, distinguish between particle ID hypotheses that overlap on the *r2p2* plot. In such cases, values of $\ln(\mathcal{L}_{\max}/\mathcal{L}_{\rm B})$ are similar and, as discussed below, D_h must be used to distinguish between hypotheses.

In the monte carlo studies performed for this note, a significance cut of $\ln(\mathcal{L}_{\max}/\mathcal{L}_{\rm B}) > 2$, corresponding to 2σ for gaussian errors, was used to estimate particle ID efficiencies. Similarly, a cut $\ln(\mathcal{L}_{\max}/\mathcal{L}_{\rm B}) < -2$ might be an appropriate indicator of a ring *not* being present in a particular search area. These cuts will have to be refined by more realistic monte carlo studies of actual physics processes.

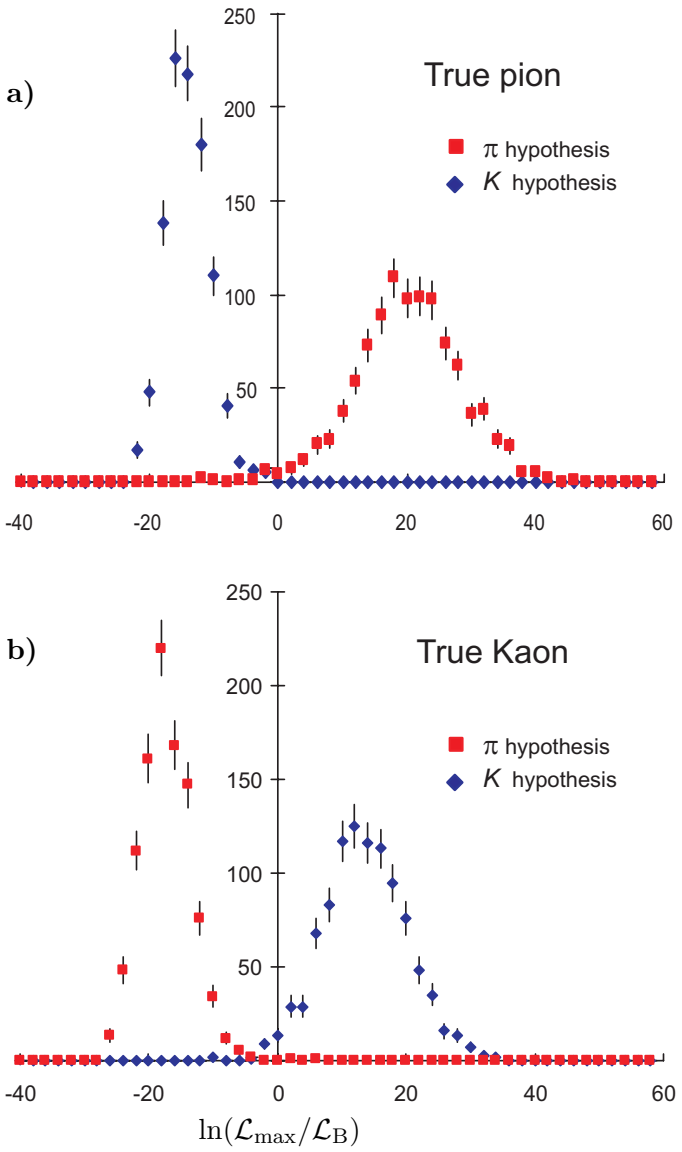

Figure 8: Results of likelihood fits using a soft momentum constraint for 20 GeV/c particles. Histogram a): number versus $\ln(\mathcal{L}_{\rm max}/\mathcal{L}_{\rm B})$ for pion and kaon hypotheses when the true particles are pions. Histogram b): number versus $\ln(\mathcal{L}_{\rm max}/\mathcal{L}_{\rm B})$ for pion and kaon hypotheses when the true particles are kaons. Fits were performed with backgrounds as depicted in Fig. 3.

7.3 Re-weighting hits on background tracks leads to marginal improvements

Because we have nearly perfect knowledge* of hits arising from background tracks in monte carlo studies, the background "re-weighting" process discussed in Sec. 4.2 can be tested by computing the corresponding background fluxes β_i from Eqn. 16 and either including it in the likelihood fits or not. We have not observed dramatic differences. In most cases, there appear to be marginal improvements in resolution, efficiency and false-ID rates when the background re-weighting is performed.

This means that it may not be necessary to perform a global re-weighting pass in most instances, thereby saving computation time. On the other hand, particular physics processes and background situations may require the best possible information from the *RICH*, in which case background re-weighting should be performed. It seems to be true that the background re-weighting is relatively more important as the average background (occupancy) increases. When actual data are studied, it may very well be necessary to perform a re-weighting pass.

Background re-weighting was performed for most of the monte carlo studies reported here. It is instructive to examine Fig. 4 where photon hits having $\beta_i \geq 10$ are distinguished from other hits, not clearly associated with background tracks. For the background conditions used in most of the studies reported here, the majority of hits are associated with other—background—tracks. Because the brightness of the target Čerenkov ring can easily exceed the β_i cut, there is still useful information contained in hits shared between the target track and other tracks.

7.4 Approximate solutions appear adequate

The approximate methods introduced in Sec. 6 for determining ring parameters and background level seem to perform adequately. Examination of single ring fits using a complete, non-linear fitting algorithm and an implementation* of the linearized approximations outlined above give results that agree within estimated errors in all cases studied. This needs to be studied more carefully with actual data.

*Smooth background described by a $R_{\rm B}$ parameter cannot be re-weighted.

*Newton's method for determining $R_{\rm B}$ is iterated until the difference is less than 1% of the estimated statistical error. This process is repeated for each iteration of ring parameters. The linearized ring-fit is iterated a fixed number of times. These approaches can be improved both for accuracy and computation time.

8 Probability Distribution for Bands on the *r2p2* Plot

In this section, we estimate the probability distribution function for deviations of data points from the ideal particle bands on the *r2p2* plot.

As discussed above in Sec. 3, in the small-angle approximation the Čerenkov relationship relating the mean Čerenkov angle $\theta_{\check{C}}$ and momentum p for a particle of mass m can be written:

$$\theta_{\check{C}}^2 = \theta_0^2 - \frac{m^2}{p^2} \qquad \theta_0^2 = 2(n-1) \tag{33}$$

where θ_0 is the "limiting" or "saturated" value of $\theta_{\check{C}}$ for speeds $\beta \to 1$.

In practice, measured values of $\theta_{\check{C}}$ (denoted* by θ) and p for a given track are compared using Eqn. 33 to find the mass hypothesis m_h that best represents the pair of measurements. Here, we assume that θ is determined by the soft momentum-constrained likelihood fitting process described in the preceeding sections. In this context, it is assumed that measured values of θ are *not* correlated with measurements of track momentum p.

We assume the track has some *true* momentum and Čerenkov angle given by $\hat{p}, \hat{\theta}$ which are related by Eqn. 33 when the correct mass hypothesis is chosen. Further, we assume the measured values p, θ are related to the true values by uncorrelated gaussian probability distributions for each variable. In particular, we assume the variables $x = (1/p^2 - 1/\hat{p}^2)/\sigma_{1/p^2}$ and $y = (\theta^2 - \hat{\theta}^2)/\sigma_{\theta^2}$† are each normally distributed with zero mean and unit variance. The respective standard deviations are related to the estimated momentum resolution $\delta p/p$ for the track and the estimated error in the determination of the Čerenkov angle $\delta\theta_{\check{C}}$ by:

$$\sigma_{1/p^2} = \frac{2}{p^2}\frac{\delta p}{p} \qquad \sigma_{\theta^2} = 2\theta\,\delta\theta_{\check{C}} \tag{34}$$

A "distance" ρ between the measured point on the *r2p2* plot and the true point can be defined by $\rho = \sqrt{x^2 + y^2}$. The most-probable estimate of $\hat{p}, \hat{\theta}$ is found by determining the *minimum* value of ρ consistent with the Čerenkov constraint (Eqn. 33). Using standard techniques, this minimum

*In the nomenclature of Sec. 4.1, $\theta = r_h + \epsilon$.

†In the limit of no background, the expected value for σ_{θ^2} is given by:$\sigma_{\theta^2} = 2\sigma/\sqrt{\mathcal{N}_0 T}$, where σ is the single photon hit angular resolution given by Eqn. 9.

distance is found to be:

$$D_h \equiv \rho_{\min} = \frac{\theta^2 - \theta_0^2 + \frac{m_h^2}{p^2}}{\sqrt{\sigma_{\theta^2}^2 + m_h^4 \sigma_{1/p^2}^2}} \tag{35}$$

where we have allowed the algebraic sign of D_h to indicate whether the measured point is above or below the band for hypothesis h. Technically, the minimum "distance" is given by $|D_h|$.

We next determine the probability distribution function for D_h (or ρ). The joint probability distribution in the variables x, y is:

$$P(x,y)\,\mathrm{d}x\,\mathrm{d}y = \frac{1}{2\pi}\mathrm{e}^{-\left(\frac{x^2+y^2}{2}\right)}\,\mathrm{d}x\,\mathrm{d}y \tag{36}$$

It is convenient to transform (x, y) to polar coordinates. The "azimuthal" coordinate is irrelevant* and can be integrated over to eliminate the factor $1/2\pi$ in the above expression. The probability distribution function in the radial coordinate ρ is given by:

$$P(\rho)\,\rho\,\mathrm{d}\rho = \mathrm{e}^{-\frac{1}{2}\rho^2}\,\mathrm{d}\left(\frac{1}{2}\rho^2\right) \tag{37}$$

This expression is easily integrated to give the probability or confidence level $\mathcal{P}(D_h)$ that the *r2p2* distance between the measured values for p, θ and the true values lies on or outside the minimum estimated distance D_h. $\mathcal{P}(D_h)$, the basic quantity being sought here, is given by:

$$\mathcal{P}(D_h) = \int_{|D_h|}^{\infty} P(\rho)\,\rho\,\mathrm{d}\rho = \mathrm{e}^{-\frac{1}{2}D_h^2} \tag{38}$$

Our approach is indicated schematically in Fig. 9. We do not *know* the true values of momentum and Čerenkov angle, $(\hat{p}\,, \hat{\theta}\,)$. We *assume* the estimated errors on the measured quantities, $(p\,, \theta)$, reflect the expected errors on $(\hat{p}\,, \hat{\theta}\,)$, at least in the vicinity of the measured point on the *r2p2* plot. Then we ask whether or not the measured point is *consistent* with the Čerenkov-constrained line of possible values for $(\hat{p}\,, \hat{\theta}\,)$ by computing $\mathcal{P}(D_h)$, the confidence level that the measured point is associated with the given *r2p2* band.

*Strictly speaking, this is true only when the resolutions σ_{1/p^2} and σ_{θ^2} do not depend on location within the *r2p2* plot. However, these quantities do depend on location, but the variations are relatively small in practice.

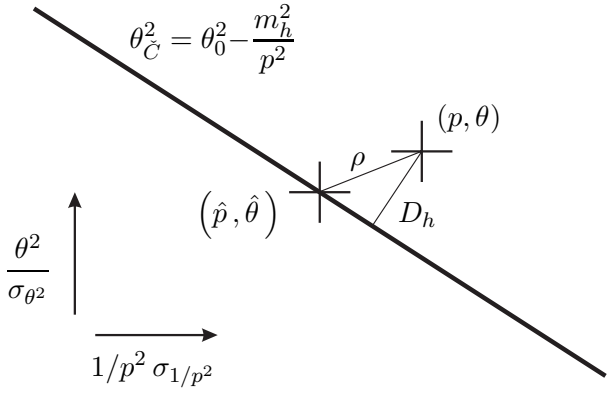

Figure 9: Schematic representation of a Čerenkov band for hypothesis h on the *r2p2* plot indicating a point at the "true" values of momentum and Čerenkov angle and a point corresponding to the measured values, (p, θ). The quantities ρ and D_h are defined in the text.

Fig. 6 shows histogram of values of D_h found from monte carlo studies discussed in Sec. 7. Notice that the mean-square value of D_h ($\langle D_h^2 \rangle \approx 2$) in the case of the correct hypothesis assignment in Fig. 6 is consistent with that expected from the definition of ρ ($\langle \rho^2 \rangle = \langle x^2 \rangle + \langle y^2 \rangle = 1 + 1$).

9 Proposed Particle ID Algorithm

Monte carlo studies described in Sec. 7 inspired a particle-ID algorithm which is outlined in this section.

The basic quantities available for selecting among the five possible hypotheses (e, μ, π, K, p) are $\ln(\mathcal{L}_{\max}/\mathcal{L}_{\rm B})$ and D_h or $\mathcal{P}(D_h)$, evaluated for each particle hypothesis h. From the discussion in Sec. 7.1 regarding the desirability of a "soft" momentum constraint, likelihood fits need be performed for single particle hypotheses only when the corresponding *r2p2* bands are distinct; when overlap occurs, it is sufficient to perform a single fit over the merged band with the soft momentum constraint.

The resulting likelihood values derived from fits to different particle bands can be compared to choose the overall most-likely hypothesis. If, on the basis of the track momentum, more than one particle band is merged in the most-likely band, then D_h can be used to derive relative probabilities for the corresponding particle hypotheses. Alternately, $\ln(\mathcal{L}_{\max}/\mathcal{L}_{\rm B})$ and D_h can be used to derive qualitative assessments of the significance

of each possible particle ID hypothesis. Comparing these assessments may yield a unique overall assignment of particle ID or not, depending on momentum, backgrounds and true particle ID. Taken together, the most-likely hypothesis and assessments of each possible ID assignment, provide different information that can be used in different ways depending on the particular physics analysis being performed.

A band-clustering algorithm was developed which merges particle hypotheses whenever their respective *r2p2* bands are within some specified distance at the measured track momentum. A useful criterion for selecting merged bands was found to be the condition that two adjacent bands are within "2+2-σ"* on the *r2p2* plot. If a third particle band satisfies this criterion with respect to the second, then all three are merged, and so on. Fig. 10 shows the bands determined for 20 Gev/c tracks.

Whenever two or more particle bands are merged, an effective mass for the band can be computed from the θ^2-coordinate of the center of the combined band and the momentum. Then, a maximum-likelihood analysis can be performed on the combined band using the single-particle methods described in Sec. 4.

Annular search areas are indicated for the methods discussed here. Center coordinates for the annulus are taken from the direction of the track being investigated. The central radius of the search area corresponds to the center of the *r2p2* band to be fitted. The width of the search area is set by the width of the *r2p2* band, to which is added $\pm n\sigma$ where σ is the single-photon hit resolution (Eqn. 9) added in quadrature with the estimated errors on track direction $\sigma_{x'}, \sigma_{y'}$. Allowance for $\pm$4-σ was chosen for the studies described here to ensure inclusion of all photons that can be expected to contribute significantly to likelihood function weights.†

Linearized likelihood fits (with the "soft" momentum constraint) are performed for each band. The results of these fits are combined in two ways to describe the particle ID content present in the data. In the first method, the band with maximum likelihood ($\ln(\mathcal{L}_{\max}/\mathcal{L}_{\mathrm{B}})$) is determined and hypotheses merged in that band are tested to find the one with the smallest value of $|D_h|$. This hypothesis is identified as the most-likely particle ID hypothesis.

The second method determines a qualitative ID assessment for every particle hypothesis that is above Čerenkov threshold. Three categories are used:

*The condition is that at least one point at the track momentum lies within 2-σ of *each* band.

†See the discussion of the parameter Δ/σ in Sec. 5.

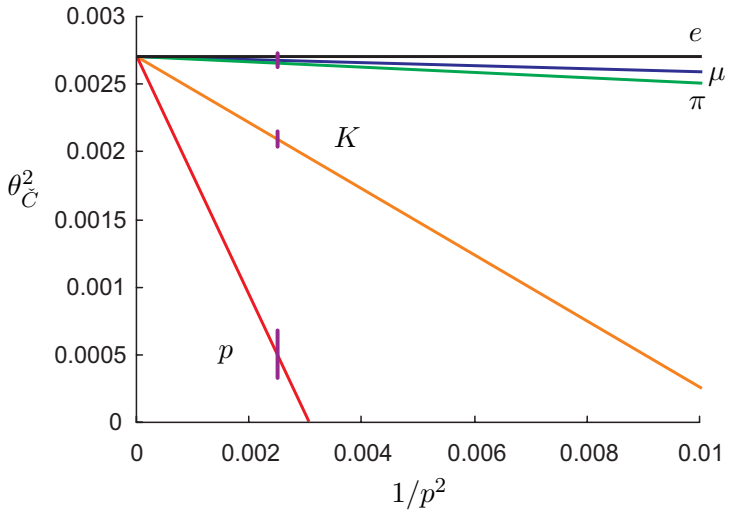

Figure 10: *r2p2* plot showing 2-σ widths of bands for a 20 GeV/c track (purple vertical lines). The e, μ, π bands are merged at this momentum.

OK indicates that the *RICH* and momentum information are fully consistent with the given particle hypothesis.

NO indicates that the data are *inconsistent* with the hypothesis.

? indicates cases that are not OK or NO.

Provisional criteria for determining particle ID categories were developed using the monte carlo tools described above. The OK category requires $\ln(\mathcal{L}_{\rm max}/\mathcal{L}_{\rm B}) > 4.5$ AND $\mathcal{P}(D_h) > 0.01$. The likelihood cut corresponds to a 3-σ significance, assuming Gaussian errors. The cut on $\mathcal{P}(D_h)$ corresponds to a 3-σ minimum distance to the particle's *r2p2* band. To be considered NO, $\ln(\mathcal{L}_{\rm max}/\mathcal{L}_{\rm B}) < 2$ OR $\mathcal{P}(D_h) < 0.001$. The likelihood cut implies that pure background is favored over the fitted ring by 2-σ and the $\mathcal{P}(D_h)$ cut says the *r2p2* coordinate falls outside 3.7 σ from the particle's band, both of which measures are indicative that the hypothesis is not likely to be correct.

Examples of these two methods for particle ID are shown in Fig. 11 for samples of 20 GeV/c monte carlo tracks that were generated as pions, kaons and protons. At this momentum, there are three bands—the e, μ, π hypotheses are merged into one. It is interesting to note that 20 GeV/c protons are barely above Čerenkov threshold ($\bar{N}_\gamma = 6.6$), yet were correctly identified as the most-likely hypothesis in all cases where they were the true particle ID; protons never indicated OK when the true particles were pions

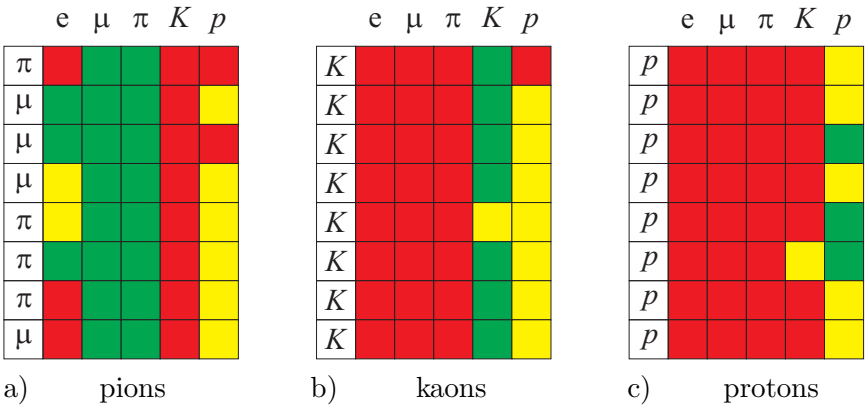

Figure 11: Results of proposed particle-ID algorithm for three sets of 20 GeV/c tracks. In the first set, labeled a), the generated tracks were pions, b) kaons and c) protons. Eight tracks are shown in each case, one row per track. The first column in each grid gives the most-likely particle hypothesis determined by the band with the largest value of $\ln(\mathcal{L}_{\max}/\mathcal{L}_{\rm B})$ and the smallest value of $|D_h|$ for hypotheses within that band. The remaining columns are color-coded to show the ID assessment for each possible hypothesis. Green indicates an "OK" rating, Red "NO" and Yellow "?". Note that at 20 GeV/c, the HERA-B *RICH* is not expected to separate electrons and pions with high reliability and protons are just above Čerenkov threshold with $\bar{N}_\gamma = 6.6$.

or kaons. Even though the HERA-B *RICH* is not expected to be able to separate pions cleanly from electrons at 20 GeV/c, electrons never faked pions as the most-likely hypothesis in the tracks shown in the figure, but muons do. Fig. 11 c) indicates that it may be possible to identify sub-threshold particles when all other hypotheses indicate NO.

How one would use the two ID methods in practice depends on the physics analysis being performed. In an analysis looking for products of the decay $D^0 \to K^-\pi^+$, for example, one may want to select kaons on the basis of the most-likely hypothesis while selecting "OK" pions. Electron and muon studies would naturally use the OK flag, unless they involve only relatively low momenta. Sub-threshold kaons or protons might be identified by requiring "NO" on competing above-threshold hypotheses.

In any event, it is important to note that the methods proposed here do not depend on any model of the underlying physics-based populations of particle types. Efficiencies and false identification probabilities need to

be estimated for the particular physics process being studied, but the basic particle ID information presented by this algorithm does not have any implicit or explicit model of particle distribution functions; it depends only on properties of the Čerenkov radiation process, masses of stable charged particles and detector performance characteristics.

10 Conclusions

We propose a particle-ID/Čerenkov ring-fitting algorithm which is well-defined mathematically, well-behaved in monte carlo simulations and which offers optimal performance over the entire *r2p2* plot, even in cases of substantial background occupancy. Monte carlo studies suggest a minor modification in approach from what was considered *a priori*—the "soft" momentum constraint—in order to eliminate undesirable correlations between fitted values of Čerenkov angle, measured values of track momenta and hypothesis mass.

Linearized fitting algorithms seem adequate, offering the possibility of substantial reductions in the computation time needed in event reconstruction.

Center coordinates of fitted Čerenkov rings provide improved resolution on the directions of the corresponding charged-particle tracks.

Values of the likelihood function and the fitted Čerenkov ring radius can be used to describe the particle-ID content present in the data for determining particle identities. We suggest two simple ways to combine this information: 1) determine the most-likely particle ID hypothesis for a given track, and 2) assess the likelihood of each possible ID hypothesis with three simple categories: "yes, no and maybe." Combining the results from these two approaches—within as little as one byte of information per track—provides useful and reliable particle ID information that can be used by *RICH* experts and non-experts for many kinds of physics analysis needs.

References

[1] R.F. Schwitters, *Rings Upon Rings: A New Approach to Pattern Recognition in Ring-Imaging Cerenkov Detectors*, Hera-B Note **HERA-B 98-088 RICH 98-006**, May 1998.

[2] R. Eckmann and D. Dujmic, *Software for Stand-alone RICH Reconstruction*, Hera-B Note **HERA-B 00-004 RICH 00-002**, January 2000.

[3] D. Dujmic, R. Eckmann and R.F. Schwitters, *Performance of the HERA-B RICH*, Hera-B Note **HERA-B 00-084 RICH 00-006**, February 2000.

[4] P. Križan and M. Starič, *An Iterative Method for the Analysis of Čerenkov Rings*, Institut "J. Stefan" Report **IJS - DP - 7819**, December 1997.

[5] Ignacio Ariño and Lluís Garrido, *Particle identification with the HERA-B RICH*, Hera-B Note **HERA-B 99-108 RICH 99-009**, July 1999.

[6] P. Baillon, *Cherenkov Ring Search Using A Maximum Likelihood Technique*, Nucl. Instr. and Methods **A238**, 341-346, 1985.

[7] J. Bächler, *et al*, *Reconstruction of Cherenkov rings in imaging detectors*, Nucl. Instr. and Methods **A343**, 273-275, 1994.

[8] U. Müller, *et al*, *Particle identification with the RICH detector in experiment WA89 at CERN*, Nucl. Instr. and Methods **A343**, 279-283, 1994.

[9] R.F. Schwitters, *Possible Instability in Classic RICH PID Algorithms*, Hera-B Note **HERA-B 00-098 RICH 00-011**, May 2000.

[10] R.F. Schwitters, *Comment on Likelihood Functions*, Hera-B Note **HERA-B 96-262 RICH 96-033**, March 1996.

[11] R.F. Schwitters, *Single-ring Likelihood Fit Including Background*, Hera-B Note **HERA-B 00-021 RICH 00-007**, March 2000.

[12] R.F. Schwitters, *"Removal" of Background Rings from Single-ring Likelihood Fits*, Hera-B Note **HERA-B 00-021 RICH 00-010**, April 2000.

[13] D. Dujmic, R. Eckmann and R.F. Schwitters, *Reconstruction of Photon Directions in the HERA-B RICH*, Hera-B Note **HERA-B 00-019 RICH 00-005**, March 1999.

[14] R.F. Schwitters, *Analytic Expression for Computing the Mean Number of Hits/Cell*, February 1997.